INDIAN JOURNAL OF SCIENCE AND TECHNOLOGY

ORIGINAL ARTICLE

Synthesis of Ti-coated Chitosan with Selenium, Zinc Oxide and Zirconium Nanocomposites by Electroplating Method: Characterizations and Biological Applications

G Kiruthiga[1], K Thanikasalam[1]*, C Pragathiswaran[1], K Selvarani[1], C Smitha[2]

1 PG and Research Department of Chemistry, Thanthai periyar Government Arts and Science College (Autonomous), Affiliated to Bharathidasan University, Tiruchirappalli - 620023, Tamil Nadu, India
2 Department of Chemistry, Government College of Engineering, Affiliated to Anna University, Srirangam Tiruchirappalli-620012, Tamil Nadu

OPEN ACCESS

Received: 07/01/2026

Accepted: 26/01/2026

Published: 05/02/2025

Citation: Kiruthiga G, Thanikasalam K, Pragathiswaran C, Selvarani K, Smitha C (2026) Synthesis of Ti-coated Chitosan with Selenium, Zinc Oxide and Zirconium Nanocomposites by Electroplating Method: Characterizations and Biological Applications. Indian Journal of Science and Technology 19(4): 215-223. https://doi.org/10.17485/IJST/v19i4.31

* **Corresponding author**.

kthanikasalam@gmail.com

Funding: None

Competing Interests: None

Published By Indian Society for Education and Environment (iSee)

ISSN
Print: 0974-6846
Electronic: 0974-5645

Abstract

Objectives: The aim of this work was to fabricate a biocompatible nanocomposite by combining titanium-coated chitosan with selenium, zinc oxide and zirconium nanoparticles through an electroplating technique to enhance biological functionality. **Methods:** Chitosan substrates were coated with titanium using electroplating followed by the incorporation of Se, ZnO and Zr nanoparticles. The resulting nanocomposites were examined using UV-Vis spectroscopy, UV-DRS, Raman spectroscopy, FT-IR and X-ray diffraction (XRD) to evaluate structural, chemical, elemental composition and morphological features. Antibacterial efficiency and cytocompatibility were assessed through in vitro biological assays. **Findings:** Characterization results confirmed the formation of a stable titanium-reinforced chitosan matrix with uniformly dispersed nanoparticles. Compared to pristine chitosan, the nanocomposite exhibited improved structural integrity and surface features. Biological studies showed a statistically significant enhancement in antibacterial and antifungal activity ($p < 0.05$) attributed to the synergistic action of Se, ZnO, and Zr nanoparticles, while maintaining high cell viability with negligible cytotoxic effects. **Novelty:** This study demonstrates a distinct electroplating-based route for integrating multiple bioactive nanoparticles into a titanium-modified chitosan framework, offering a multifunctional biomaterial with enhanced antimicrobial efficacy and preserved cytocompatibility for biomedical applications.

Keywords: Chitason; Titanium; Selenium; Zirconium and ZnO nanoparticles; UV; UV-DRS; XRD and FTIR

1 Introduction

The development of multifunctional biomaterials with enhanced mechanical stability, antimicrobial activity, corrosion resistance and biocompatibility has gained increasing attention due to their wide potential in biomedical and healthcare applications [1]. Among naturally derived polymers, chitosan has emerged as a promising material owing to its biodegradability, biocompatibility, non-toxic and inherent antimicrobial properties. Chitosan is a natural polysaccharide obtained from chitin, which is abundantly present in the exoskeletons of shellfish, insects and fungal sell walls [2], [3]. Owing to the presence of amino and hydroxyl group, Chitosan (CS) can act as reducing and capping agent during nanocomposite synthesis. The Primary amine groups impart a positive charge to chitosan enabiling strong electrostatic interactions with negatively charged biological surfaces and providing enhanced stability to chitosan-based matrics [4].

Based on their electronegativity behaviour, chitosan can effectively facilitate the formation of nanocomposites. However, pristine chitosan exhibit poor mechanical strength and limited functional stability which can restrict its use in demanding applications such wound dressings, implant coatings and tissue engineering scaffolds [5]. To address these limitations, extensive efforts have been directed toward incorporating inorganic nanomaterials into chitosan matrices to synergistically improve mechanical integrity, antimicrobial performance and corrosion protection [6], [7], [8]. Zinc oxide (ZnO) nanoparticles have attracted significant attention due to their broad-spectrum antibacterial activity, corrosion inhibition capability and ability to promote cell proliferation [9], [10]. Recent studies have demonstrated that ZnO-reinforced chitosan composites exhibit enhanced antibacterial efficacy, improve corrosion resistance and superior biocompatibility, making them suitable for wound healing and implant surface coatings [11], [12]. Selenium nanoparticles are recognized for their antioxidant and antimicrobial behavior [13] while Zirconium-based materials contribute to improved mechanical stability, wear resistance, and corrosion resistance along with excellent biocompatibility [14]. The synergistic integration of these nanoparticles within a chitosan–titanium matrix is therefore expected to generate a multifunctional nanocomposite with superior physicochemical, electrochemical and biological performance [15], [16].

Despite numerous reports on chitosan-based nanocomposites, studies focusing on the combined incorporation of selenium, zinc oxide, and zirconium nanoparticles within a titanium-coated chitosan framework using electrochemical deposition methods [17], [18]. Electroplating offers a controlled approach to achieving uniform coatings with strong interfacial adhesion and tunable surface features [19], [20]. The present work addresses this research gap by developing Ti-coated chitosan nanocomposites embedded with selenium, ZnO, and zirconium nanoparticles via electroplating and evaluating their coating stability, structural and surface characteristics using UV-Vis spectroscopy, UV-DRS, Raman spectroscopy, FT-IR and X-ray diffraction (XRD). The outcomes of this study aim to provide valuable insights into the design of advanced nanocomposite biomaterials for antimicrobial and biomedical applications.

2 Methodology

In this work, titanium sheet has been selected among the measurements of 40mm length, 10mm breadth and 1mm thickness. The test sample was prepared using analytical grades chemicals. Sigma-Aldrich delivered Chitosan (deacetylation degree >75%).

2.1 Synthesis of CS/Se, CS/ZnO and CS/Zr Nanoparticles by Electrodeposition Method

Electroplating is a widely used metal deposition technique in which an electrolyte medium is employed to form a uniform coating on a substrate. The selection of appropriate process parameters is critical to achieving high-quality and adherent coatings. Prior to electroplating, the titanium specimens were mechanically polished using emery sheets to enhance surface roughness and improve coating adhesion. Hank's solution was used as the electrolyte medium in this study due to its physiological relevance. Hank's solution is a buffered salt solution rich in bicarbonate ions and is commonly used in cell culture systems to maintain stable pH conditions. The solution was prepared by dissolving NaCl (8 g), KCl (0.4 g), $CaCl_2$ (0.14 g), $MgSO_4$ (0.06 g), $MgCl_2$ (0.1 g), Na_2HPO_4 (0.06 g), KH_2PO_4 (0.06 g), $NaHCO_3$ (0.35 g), and D-glucose (1 g) in 1 L of distilled water.

The electroplating experiments were carried out using a potentiostat/galvanostat equipped with an impedance analyzer (Model 73022, Autolab Instruments, Metrohm) in a conventional three-electrode electrochemical cell at 36 °C. The titanium substrate served as the working electrode with an exposed area of 0.1 cm^2, a saturated calomel electrode (SCE) was used as the reference electrode, and a platinum wire acted as the counter electrode. Potentiodynamic polarization measurements were performed in the potential range of −0.5 to +1.5 V versus SCE at a scan rate of 50 mV s^{-1}. Experiments were conducted at different coating concentrations, as summarized in Table 1.

Table 1. Electroplating Process Parameters

Sl. No.	Input parameters	Units	Levels
1.	Chitosan	Gram	0.4
2.	Selenium	Gram	0.2
3.	Zinc Oxide	Gram	0.2
4.	Zirconium	Gram	0.2

3 Results and Discussion

3.1 Characterization Of Cs/Se, Cs/Zno And Cs/Zr Nanocomposite

3.1.1. Uv-Visible Spectral Analysis

The UV–Vis spectral behavior observed in this study demonstrates enhanced optical modification of chitosan upon nanoparticle incorporation compared with previously reported ZnO–chitosan systems developed for drug delivery[(2)]. In a weakly acidic medium, chitosan exhibits a characteristic absorption band associated with surface plasmon resonance around 330 nm. While earlier studies reported absorption bands in the 350–380 nm range corresponding to ZnO–chitosan interactions, the CS/ZnO nanocomposite deposited on a titanium substrate in the present work exhibited a pronounced red shift to approximately 420 nm as shown in Figure 1(i). This larger shift indicates stronger electronic coupling and improved nanoparticle dispersion facilitated by the electrochemical deposition process. In addition, the observed peak shifts for CS/Se (350 to 360 nm) in Figure 1(ii) and CS/Zr (230 to 310 nm) in Figure 1(iii) further confirmation of the successful formation of multi-nanoparticle chitosan composites. These characteristic peak shifts clearly indicate the successful formation of CS/Se, CS/ZnO, and CS/Zr nanocomposites on the titanium substrate, as confirmed by UV–Vis spectral analysis.

Overall, the UV–Vis results highlight the advantage of the titanium-supported electrochemical approach in achieving enhanced interfacial interactions and broader functional versatility compared to previously reported chitosan-based nanocomposites.

3.1.2. Uv–Visible Diffuse Reflectance Spectra [UV-DRS] Investigation

UV-Visible diffuse reflectance spectroscopy (DRS) was employed to characterize the optical properties of the solid particularly optically rough films and powder-based materials. The incorporation of selenium, Zinc oxide and Zirconium nanoparticles into the chitosan matrix resulted in distinct change in the reflectance spectra. Pure chitosan exhibited an absorption edge around 300–350 nm, whereas the CS/Se nanocomposite showed a pronounced red shift to approximately 470 nm. Similarly, the characteristic absorption band of chitosan at about 350 nm shifted to nearly 400 nm upon the incorporation of ZnO nanoparticles, while the CS/Zr nanocomposite displayed a shift toward approximately 500 nm. These spectral shifts confirm the successful formation of CS/Se, CS/ZnO, and CS/Zr nanocomposites, as shown in Figure 1(iv–vi).

The optical band gap energies were estimated using the Kubelka–Munk function. The calculated band gap values were approximately 3.6eV for pristine chitosan and 2.43eV for CS/Se, 3.6eV and 3.1eV for chitosan and CS/ZnO, respectively, and 3.6eV and 4.0eV for chitosan and CS/Zr. The observed reduction and variation in band gap energies can be attributed to the incorporation of small amounts of Se, ZnO, and Zr nanoparticles into the chitosan matrix deposited on the titanium surface, which modifies the electronic structure of the composites.

3.1.3. X-Ray Diffraction (XRD)

The X-ray diffraction (XRD) analysis revealed that the chitosan/selenium (CS/Se) and chitosan/zinc oxide (CS/ZnO) nanocomposites exhibited well-defined crystalline structures. All diffraction peaks observed in the XRD patterns showed excellent agreement with the corresponding standard data from the Joint Committee on Powder Diffraction Standards (JCPDS) files, confirming phase purity and the absence of detectable impurities. The XRD patterns of chitosan incorporated with Se, ZnO, and Zr nanoparticles deposited on the titanium substrate under optimized conditions are presented in Figure 2(vii–ix).

The CS/Se nanocomposite exhibited three prominent diffraction peaks at 2θ values of approximately 20°, 24°, and 44°, corresponding to the (222), (012), and (011) crystallographic planes, respectively (JCPDS card no. 88-0618). Similarly, the CS/ZnO nanocomposite showed major reflections indexed to the (211), (220), and (200) planes, confirming the crystalline nature of ZnO within the chitosan matrix. For the CS/Zr nanocomposite, sharp diffraction peaks were observed at 2θ values near 45°, 54°, and 57°, corresponding to the (100), (110), and (012) planes, respectively, in agreement with standard JCPDS data.

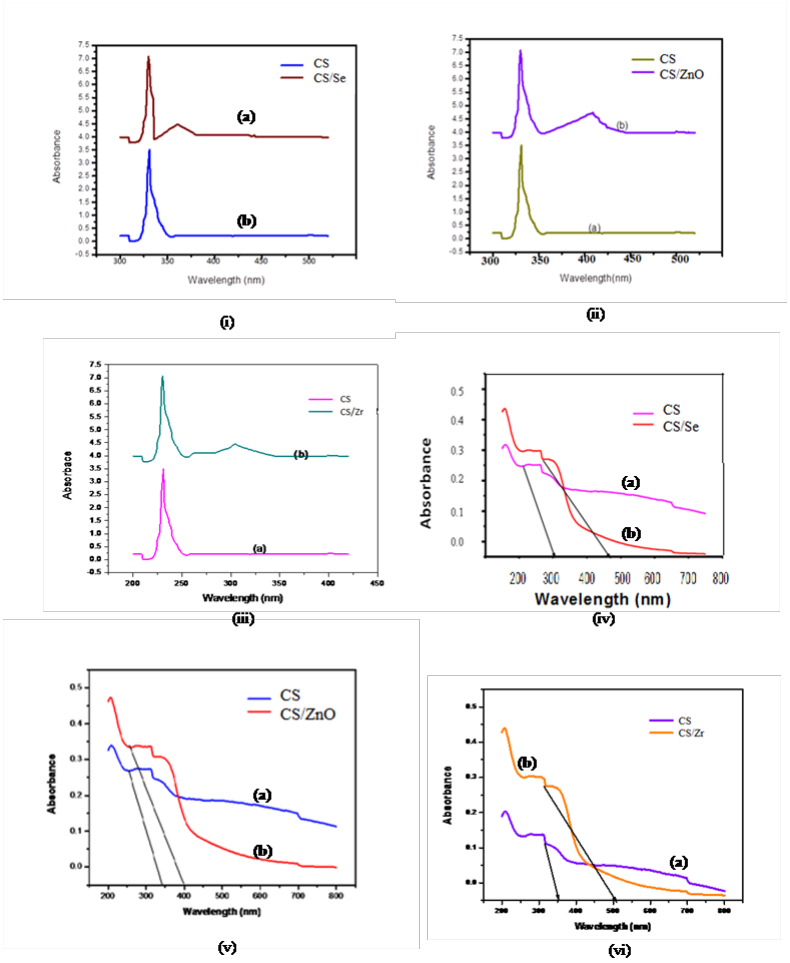

Fig 1. In (i), (ii), (iii) UV-Visible spectrum of (a) CS and (b) CS/Se, CS/ZnO and CS/Zr nanocomposite. In (iv), (v), (vi) UV-DRS Spectrum of (a) CS and (b) CS/Se, CS/ZnO and (b) CS/Zr nanocomposite.

The presence of characteristic diffraction planes such as (011), (220), and (110) confirms the successful coordination and uniform distribution of selenium, zinc oxide, and zirconium nanoparticles within the chitosan biopolymer matrix. The crystallite sizes were calculated using the Debye–Scherrer equation ($D = K\lambda/\beta\cos\theta$). Pristine chitosan exhibited an average crystallite size in the range of 11–13.1 nm, while nanoparticle incorporation increased the crystallite size to approximately 17 nm for CS/Se, 16.2 nm for CS/ZnO, and 15.2 nm for CS/Zr. This increase indicates enhanced crystallinity and structural ordering induced by nanoparticle integration. Unlike earlier reports that frequently describe nanoparticles agglomeration within chitosan matrices[20]. The present system exhibits well-defined hexagonal crystalline structures, highlighting the effectiveness and novelty of the electrochemical deposition approach.

3.1.4. Fourier Transform Infrared (FT-IR) Analysis.

Fourier transform infrared (FTIR) spectroscopy was used to analyze the functional groups of chitosan (CS) and its nanocomposites, as shown in Figure 2(x–xii). The FTIR results obtained in this study are consistent with previously reported biopolymer–metal nanocomposite systems, while also demonstrating distinct interaction features arising from the chitosan matrix and electrochemical deposition method. In the study on T. terrestris incorporated titanium-doped ZnO/cellulose nanocomposite films[15], characteristic cellulose bands associated with O–H stretching and C–O–C vibrations were retained after nanoparticle incorporation, with slight band shifts attributed to hydrogen bonding and metal–polymer coordination. Similar retention of polymer backbone vibrations was observed in the present work, where the characteristic O–H, N–H, and amide I bands of chitosan remained prominent, indicating preservation of the biopolymer framework.

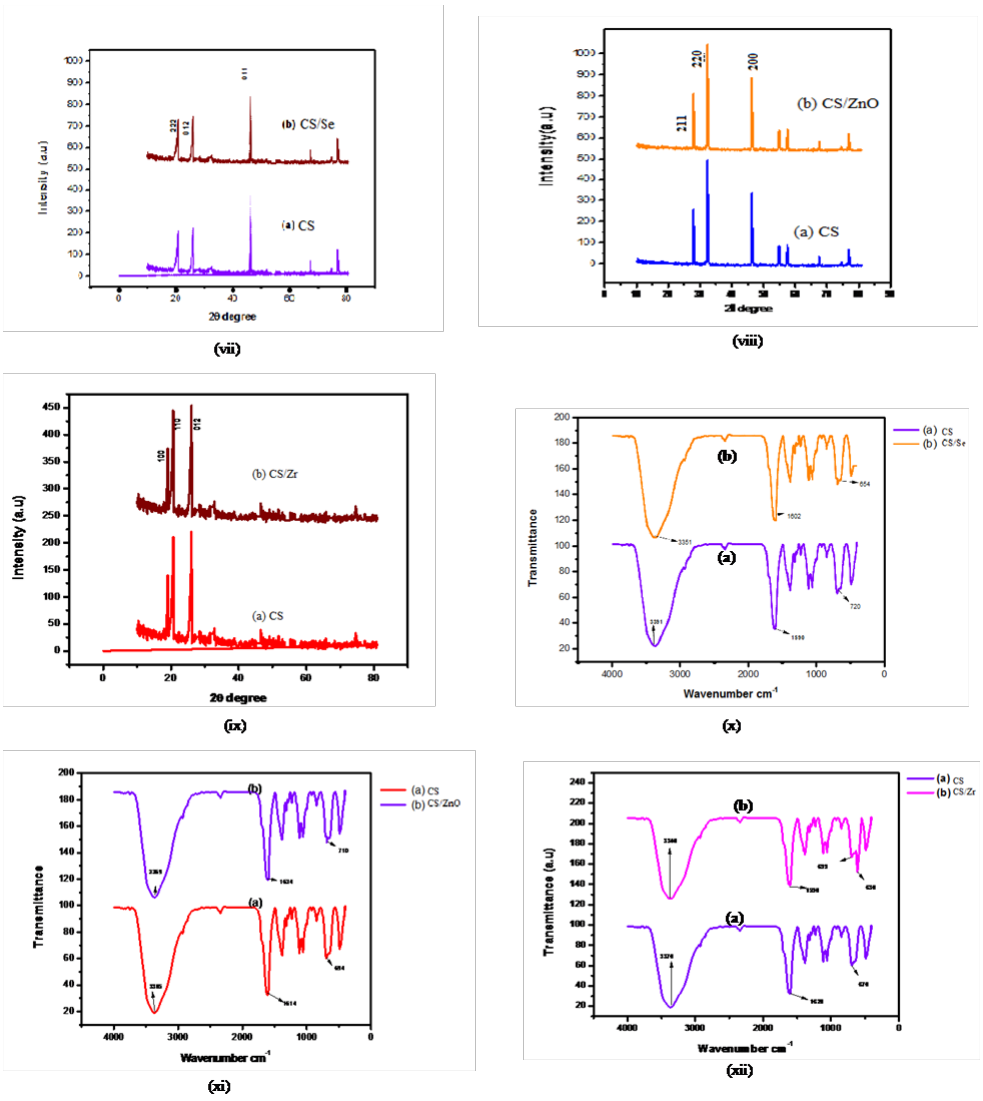

Fig 2. In (vii), (viii), (ix) XRD spectrum of (a) CS and (b) CS/Se, CS/ZnO and CS/Zr nanocomposite. In (x), (xi), (xii) FT-IR Spectrum for (a) CS and (b) CS/Se, CS/ZnO and (b) CS/Zr nanocomposite.

However, compared to cellulose-based systems, the chitosan nanocomposites exhibited more pronounced band shifts in the low-frequency region (650–720 cm^{-1}), reflecting stronger coordination interactions between metal nanoparticles and chitosan functional groups such as amine and hydroxyl moieties. The observed shifts for CS/Se (720 cm^{-1} shifted to 654 cm^{-1}), CS/ZnO (694 cm^{-1} to 720 cm^{-1}), and CS/Zr (670 cm^{-1} to 699 cm^{-1}) nanocomposites suggest enhanced metal–ligand interactions relative to previously reported ZnO–cellulose composites. This enhanced interaction is attributed to the presence of both amine and hydroxyl functional groups in chitosan, which promotes improved nanoparticle stabilization and interfacial bonding.

3.1.5. Corrosion Studies

In this study, corrosion [6], [9] inhibition performance of the CS/Se, CS/ZnO and CS/Zr nanocomposite coated on titanium was evaluated using weight loss measurement, cyclic voltametry, electrochemical impedence spectroscopy and potentiodynamic polarization techniques. In this experimental investigation, a titanium sheet with dimension of 40mm × 10mm × 1mm were selected and the weight of the selected specimen was measured by using Denver analytical balance (Germany). Solutions such as acidic, alkaline, neutral and Hank's solutions were extensively included to accelerate the presence of corrosion on the material surface.

As this work aims to explore titanium-based materials for bone replacement applications, Hank's solution was selected as the reference (blank) electrolyte to simulate physiological conditions. The titanium specimens were immersed in 100 mL of Hank's solution for a duration of 144 hours to evaluate the corrosion rate. The corresponding corrosion data obtained from the weight loss measurements are presented in Table 2.

Table 2. Corrosion rate of CS/Se, CS/ZnO and CS/Zr

Nanocomposite	Weight(mg)	Corrosion Inhibition Efficiency(%)	Corrosion rate
CS/Se	0.4	96	0.0056
CS/ZnO	0.4	99	0.0056
CS/Zr	0.4	98	0.0056

3.1.6. Electrochemical Impedence Spectroscopy (EIS)

Nyquist plots of chitosan-coated titanium immersed in Hank's solution, both in the absence and presence of SeNPs, ZnONPs, and ZrNPs coatings, are shown in **Figures 3**(xiii–xv)**.** The Nyquist plots were used to evaluate key impedance parameters, including the charge transfer resistance (Rct) and double layer capacitance (Cdl). For chitosan-coated titanium, the Rct and Cdl values were found to be approximately 125 $\Omega{\cdot}cm^2$ and 78 $\mu F/cm^2$, respectively.

Upon incorporation of nanoparticles, a significant increase in Rct and a corresponding decrease in Cdl were observed. Specifically, the Rct value increased from 125 to 810 $\Omega{\cdot}cm^2$ for CS/Se, from 125 to 900 $\Omega{\cdot}cm^2$ for CS/ZnO, and from 125 to 812 $\Omega{\cdot}cm^2$ for CS/Zr coatings. Simultaneously, the Cdl values decreased from 78 to 4.6 $\mu F/cm^2$ for CS/Se, to 4.1 $\mu F/cm^2$ for CS/ZnO, and to 4.6 $\mu F/cm^2$ for CS/Zr. The increase in Rct combined with the reduction in Cdl indicates enhanced surface protection and increased interfacial stiffness due to the formation of a stable electrical double layer on the titanium surface. The variation of Rct with Cdl values is summarized in Table 3.

Table 3. Electrochemical Impedances

Electrodes	Charge Transfer Resistance R_{ct} (Ωcm^2)	Double Layer Capacitance ZnO ($\mu F/cm^2$)	IE_{imp} (%)
Ti	125	78	90
Ti-CS/Se	810	4.6	99
Ti-CS/ZnO	900	4.1	99
Ti-CS/Zr	950	3.8	98

3.1.7. Potentiodynamic Polarization

Potentiodynamic polarization measurements were carried out to obtain a detailed assessment of the corrosion behavior of nanoparticle-coated titanium in Hank's solution. The polarization curves were recorded by scanning the potential from −0.5 to +1.5 V versus the saturated calomel electrode (SCE) at a scan rate of 50 mV s^{-1}. The corresponding electrochemical parameters and inhibition efficiencies are summarized in Table 4.

Table 4. Corrosion Parameters in Hank's Solution

Electrodes	**Corrosion potential (mV)**	**Current density($\mu A/cm^{-2}$)**	**Anodic Tafel slope (mV/dec^{-1})**	**Cathodic Tafel slope (mV/dec^{-1})**	**CIE(%)**
Ti	-512	2.29	77	238	90
Ti-CS/Se	-469	74.60	117.95	210.70	99
Ti-CS/ZnO	-490	1.16	270	285	99
Ti-CS/Zr	-426	1.16	333	166	98

The corrosion potential (E_{corr}) and corrosion current density (i_{corr}) were determined using the Tafel extrapolation method. Compared to uncoated titanium, the nanoparticle-coated samples exhibited a positive shift in E_{corr} and a significant reduction in i_{corr}, indicating enhanced corrosion resistance. The anodic and cathodic Tafel slopes remained nearly constant for all coatings, suggesting that the corrosion mechanism was not significantly altered. Among the coatings, CS/Se exhibited the

lowest i_{corr} and the most positive E_{corr}, indicating superior corrosion protection. Corrosion inhibition efficiencies calculated from icorr values were found to be approximately 99% for CS/Se and CS/ZnO, and 98% for CS/Zr, corroborating the impedance results.

These findings indicate that the nanocomposite coatings predominantly suppress anodic dissolution while also influencing cathodic reactions, leading to the formation of a stable protective layer on the titanium surface. The polarization behaviors of the coated samples are shown in Figure 3(xvi-xviii).

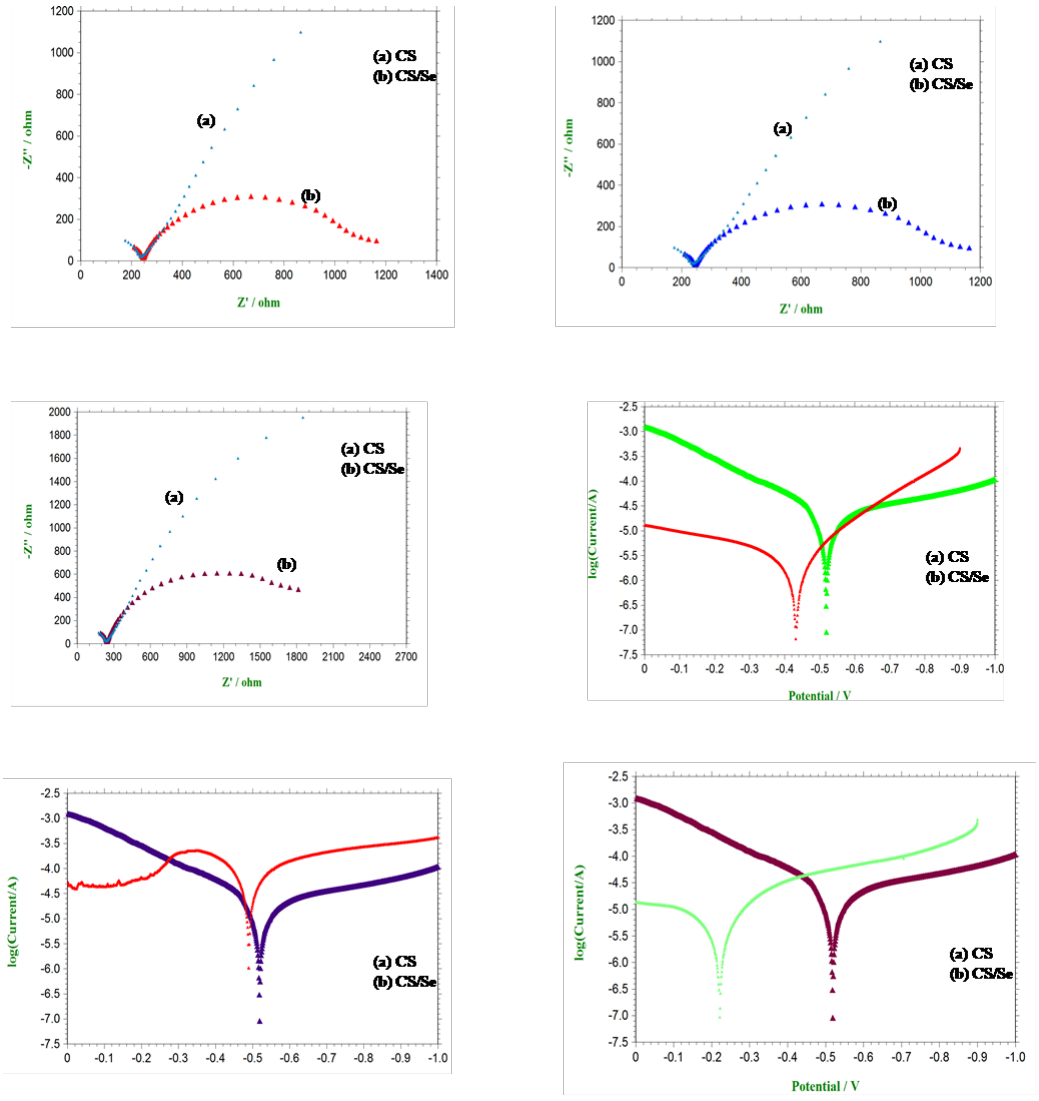

Fig 3. In (xiii), (xiv), (xv) EIS spectrum for (a) CS and (b) CS/Se, CS/ZnO and CS/Zr nanocomposite. In (xvi), (xvii), (xviii) Potentiodynamic polarization of (a) CS and (b) CS/Se, CS/ZnO and (b) CS/Zr nanocomposite.

3.1.8. Biological Application

The antifungal activity of CS/Se, CS/ZnO, and CS/Zr nanocomposites against *Candida albicans* is presented in Tables 5– 7. All samples exhibited a concentration-dependent response. Pristine chitosan showed weak antifungal activity, with inhibition zones increasing marginally from 0 to 3 mm as the concentration increased from 20 to 100μg/ml. In contrast, all nanocomposite coatings demonstrated enhanced antifungal performance at corresponding concentrations. Detectable inhibition ($\approx$1 mm) was observed for all nanocomposites even at low concentrations (20–40 μg/ml), where pristine chitosan remained largely inactive.

Table 5. Antifungal activity of CS and CS/Se nanocomposite

Nanocomposites	Concentrations (μg/ml)	Organism/zone of inhibition(mm) *Candida albicans*	
		CS	CS/Se
	20	0	1
40	1	1	
Samples	60	1	3
80	2	4	
100	3	5	
Control G (glacial acetic acid)	10μl/disc	0	0

Table 6. Antifungal activity of CS and CS/ZnO nanocomposite

Nanocomposites	Concentrations (μg/ml)	Organism/zone of inhibition(mm) *Candida albicans*	
CS	CS/ZnO		
	20	0	1
	40	1	1
Samples	60	1	2
	80	2	4
	100	3	4
Control G (glacial acetic acid)	10μl/disc	0	0

Table 7. Antifungal activity of CS and CS/Zr nanocomposite

Nanocomposites	Concentrations (μg/ml)	Organism/zone of inhibition(mm) *Candida albicans*	
		CS	CS/Zr
	20	0	1
	40	1	1
Samples	60	1	3
	80	2	4
	100	3	6
Control G (glacial acetic acid)	10μl/disc	0	0

At 100μg/ml, inhibition zones of 5 mm and 4 mm were recorded for CS/Se and CS/ZnO, respectively, while CS/Zr exhibited the highest activity with a maximum inhibition zone of 6 mm. The control (glacial acetic acid) showed no inhibitory effect.

The improved antifungal performance of the nanocomposites compared to pristine chitosan confirms the beneficial role of metal nanoparticle incorporation. Compared with previously reported[17] chitosan/ZnO systems that primarily emphasized antibacterial effects at higher ZnO loadings, the present coatings exhibit a stronger and more consistent antifungal response against *Candida albicans*, including activity at lower concentrations. Among the formulations, CS/Zr showed superior efficacy, followed by CS/Se and CS/ZnO. Overall, the antifungal effectiveness followed the order: CS/Zr > CS/Se > CS/ZnO > CS. This enhancement is attributed to synergistic mechanisms involving disruption of fungal cell wall integrity, increased reactive oxygen species generation, release of metal ions, and increased membrane permeability, collectively leading to effective inhibition of fungal growth.

4 Conclusion

The present study successfully demonstrates the fabrication of chitosan-based bio-nanocomposite coatings containing selenium, zinc oxide, and zirconium nanoparticles on titanium substrates using an electrochemical deposition technique. UV–visible and UV–DRS analyses confirmed nanoparticle incorporation through characteristic absorption bands and reduced band gap energies. XRD results revealed the crystalline nature and hexagonal structure of CS/Se, CS/ZnO and CS/Zr nanocomposites, while FT-IR analysis verified strong coordination between chitosan functional groups and the embedded nanoparticles.

Electrochemical corrosion measurements in Hank's solution revealed outstanding protective performance, with inhibition efficiencies reaching 99% for CS/Se and CS/ZnO and 98% for CS/Zr, attributed to the formation of a dense and adherent barrier layer. Increased charge transfer resistance and decreased double-layer capacitance confirmed the formation of a compact and stable protective layer on titanium.

The antifungal results confirm that nanoparticle-modified chitosan exhibits significantly enhanced activity against *Candida albicans* compared to pristine chitosan. Among the formulations, CS/Zr showed the highest inhibition followed by CS/Se and CS/ZnO, demonstrating a clear concentration-dependent response. These findings emphasize the effectiveness of metal nanoparticle incorporation in improving the antifungal performance of chitosan-based biomaterials. Overall, the combined corrosion protection and antifungal performance highlight the potential of these multifunctional chitosan-based nanocomposite coatings for biomedical and implant-related applications.

References

1) Chen MC, Koh PW, Ponnusamy VK. Titanium dioxide and other nanomaterials based antimicrobial additives in functional paints and coatings: Review. *Progress in Organic Coatings*. 2022;163:106660.
2) Ghalee-taki GN, Rastegari AA, Hekmat A. Synthesis and characterization of zinc oxide-chitosan nanocomposite for targeted drug delivery to the colon. *BioNanoScience*. 2024;24:2337–2364. 10.1007/s12668-024-01476-z.
3) Mawazi SM, Kumar M, Ahmad N, Ge Y, Mahmood S. Recent applications of chitosan and its derivatives in antibacterial, anticancer, wound healing, and tissue engineering fields. *Polymers*. 2024;16(10):1351. 10.3390/polym16101351.
4) Sathiyaseelan A, Naveen KV, Zhang X, Han K, Wang MH. Research progress on chitosan-zinc oxide nanocomposites fabrication, characterization, biomedical and environmental applications. *Coordination Chemistry Reviews*. 2023;496. 10.1016/j.ccr.2023.215398.
5) Pragathiswaran C, Thulasi G, Al-Ansari MM, Al-Humid, Saravanan M. Experimental Investigation and Electrochemical characterization of titanium coated nanocomposite materials for biomedical applications. *Journal of Molecular Structure*. 2021;1231:129932.
6) Pragathiswaran C, Ramadevi P, Kumar KK. Imidazole and Al3+ nano material as corrosion inhibitor for mild steel in hydrochloric acid solutions. *Materials Today: Proceedings*. 2021;37:2912–2916.
7) Al-Rajhi AMH, Abdelghany TM, Almuhayawi MS, et al. The green approach of chitosan/Fe2O3/ZnO-nanocomposite synthesis with an evaluation of its biological activities. *Applied Biological Chemistry*. 2024;67(75). 10.1186/s13765-024-00926-2.
8) Kalairasi J, Balakrishnan D. Sensing and antimicrobial activity of polyaniline doped with TiO2 nanocomposite synthesis and characterization. *Journal of King Saud University - Science*. 2022;34(3):101824.
9) Thulasi G, Pragathiswaran C. Experimental investigation and analysis of corrosion inhibition of titanium modified by chitosan silver nanomaterials and its applications. *Materials Today: Proceedings*. 2021;37:2780–2785.
10) Amiri MR, Alavi M. Antibacterial, antifungal, antiviral, and photocatalytic activities of TiO2 nanoparticles, nanocomposites, and bio-nanocomposites: Recent advances and challenges. *Journal of Public Health Research*. 2022;11.
11) Anusuya N, Pragathiswaran C, Mary JV. A potential catalyst-TiO2/ZnO based chitosan gel beads for the reduction of nitro-aromatic compounds aggregated sodium borohydride and their antimicrobial activity. *Journal of Molecular Structure*. 2021;1236.
12) Azmana M, Mahmood S, Hilles AR. A review on chitosan and chitosan-based bionanocomposites: Promising material for combating global issues and its applications. *International Journal of Biological Macromolecules*. 2021;185.
13) Ruan Q, Yuan L, Gao S. Selenium-based chitosan nanocomposites: antioxidant and antimicrobial activities for biomedical use. *International Wound Journal*. 2023;20(6):1819–1831. 10.1111/iwj.13984.
14) Nagaraj K, Kaliyaperumal R, Poovan VK. Zirconium-doped zinc nanocomposites (ZDZN): Preparation, characterization and evaluation of antibacterial activity. *Journal of the Indian Chemical Society*. 2021;101(11):101386. 10.1016/j.jics.2024.101386.
15) Bahadur GCR, Awasthi GP, Shin M, et al. Fabrication, characterization and Biological evaluation of T. Terrestris incorporated Titanium-doped ZnO/cellulose nanocomposite films as a therapeutic hemostatic scaffold for diabetic wound healing. *ACS Omega*. 2024;9(16):18327–18340. 10.1021/acsomega.4c00174.
16) Bashal AH, Riyadh SM, Alharbi W, Alharbi KH, Farghaly TA, Khalil KD. Bio-Based (chitosan-ZnO) nanocomposite: Synthesis, characterization and its use as recyclable, ecofriendly biocatalyst for synthesis of Thiazoles tethered Azo groups. *Polymers*. 2022;14(3):386. 10.3390/polym14030386.
17) Ali SA, Ali ES, Hamdy G, et al. Enhancing physical characteristics and antibacterial efficacy of chitosan through investigation of microwave-assisted chemically formulated chitosan-coated ZnO and chitosan/ZnO physical composite. *Scientific Reports*. 2024;14:9348. 10.1038/s41598-024-58862-6.
18) Abdellatif AS, Shahien M, El-saeed AM. Titanate-polyurethane-chitosan ternary nanocomposites as an efficient coating for steel against corrosion. *Scientific Reports*. 2024;14:30562. 10.1038/s41598-024-81104-8.
19) Joseph DS, Nallaswamy S, Rajeskumar P, Dathan L, Jose L. A comprehensive review of synthesis, properties and application of TiO2 and ZnO nanoparticles. *Journal of Clinical and Diagnostic Research*. 2024;18(5):ZE05–ZE10. 10.7860/JCDR/2024/69854.19399.
20) Safari P, Rahimabadi EZ, Vaezi MR, Behnamghader A. Development of ZnO-NPs reinforced chitosan nanofiber mats with improved antibacterial and biocompatibility properties. *Scientific Reports*. 2025;15:16567. 10.1038/s41598-025-01669-w.